B-T-3287

THEORY AND APPLICATION OF DETERMINISTIC, MULTIDIMENSIONAL, POINTWISE ENERGY LATTICE PHYSICS METHODS

M. L. Zerkle

Contract No. DE-AC11-98PN38206

BETTIS ATOMIC POWER LABORATORY WEST MIFFLIN, PENNSYLVANIA 15122-0079

Operated for the U. S. Department of Energy
by Bechtel Bettis, Inc.

THEORY AND APPLICATION OF DETERMINISTIC, MULTIDIMENSIONAL, POINTWISE ENERGY LATTICE PHYSICS METHODS

M. L. Zerkle
Bettis Atomic Power Laboratory
P.O. Box 79
West Mifflin, PA 15122-0079
(412) 476-6188

ABSTRACT

The theory and application of deterministic, multidimensional, pointwise energy lattice physics methods are discussed. These methods may be used to solve the neutron transport equation in multidimensional geometries using near-continuous energy detail to calculate equivalent few-group diffusion theory constants that rigorously account for spatial and spectral self-shielding effects. A dual energy resolution slowing down algorithm is described which reduces the computer memory and disk storage requirements for the slowing down calculation. Results are presented for a 2D BWR pin cell depletion benchmark problem.

I. INTRODUCTION

This paper describes methods that are being developed to generate transport corrected few-group diffusion theory constants for diffusion theory programs such as PDQ08.[1] These methods solve the neutron transport equation in one- and two-dimensional geometries using a near-continuous energy pointwise solution procedure that rigorously accounts for the effects of spatial and spectral self-shielding. In our work, a weighted diamond difference or a method of characteristics scheme is used for the spatial solution of the discrete ordinates transport equations. A dual energy resolution slowing down algorithm is used to reduce the computer memory and disk storage requirements of the slowing down calculation while retaining most of the accuracy of the detailed pointwise energy solution. The near-continuous energy transport solution for a detailed transport theory geometry is collapsed to few-groups and homogenized over a coarser corresponding diffusion theory geometry. An iterative normalization (fitting) algorithm is used to generate equivalent few-group diffusion theory constants that reproduce the few-group reaction rates of the homogenized transport solution within user specified criteria.

Traditional multidimensional lattice physics methods, such as those used in the CASMO[2] and CPM[3] codes, use an interface current or a WIMS[4] type method of characteristics transport solver, multigroup cross sections, and assume isotropic scattering in the Laboratory system. Our pointwise solution method uses significantly more energy, spatial, and angular detail than the methods used in traditional lattice physics codes to more accurately represent spatial and spectral shelf-shielding effects throughout life. The CENTRUM[5] code uses a similar pointwise energy solution method. In this paper, we reserve the term "pointwise" for treatments that discretize the energy domain into 1000s to 10,000s of energy intervals and use cross sections at discrete energy points obtained directly from a continuous energy cross section library. This is to be distinguished from "multigroup" treatments that typically discretize the energy domain into 10s to 100s of energy groups and use group-averaged cross sections that are generated by an energy collapsing procedure. The term "near-continuous energy" is used for pointwise treatments that have an energy detail approaching that of the continuous energy cross section library.

II. CALCULATION OVERVIEW

As illustrated in Figure 1, the calculational procedure contains five main solution modules: the pointwise energy transport solution module, a diffusion theory solution module, a few-group cross section fitting module, a few-group diffusion theory parameter output module, and a depletion module. The transport solution module uses a near-continuous energy solution method to solve the neutron transport equation over a detailed transport theory cell geometry. Nuclear data for the transport solution is provided by an ultra-fine, Doppler broadened, pointwise cross section library generated by the RCPL1 program.[6] These RCPL1 libraries typically contain over 40,000 energy points in the fast energy range and 300 energy points in the ther-

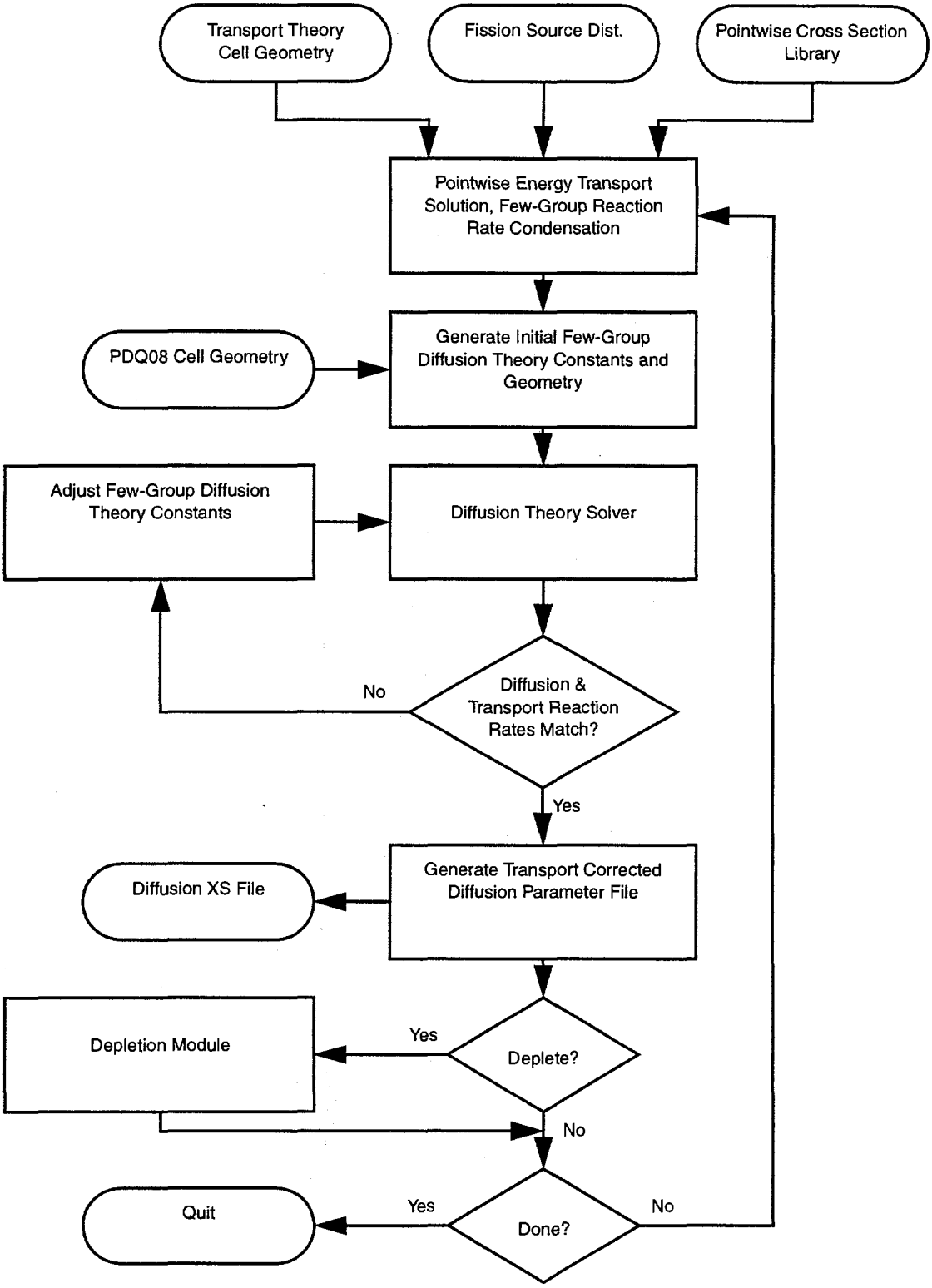

Figure 1. Calculational Flowchart

mal energy range. In order to limit the error associated with the fixed source approximation, a fission source distribution from a companion RCP01[7] continuous energy Monte Carlo eigenvalue calculation may be used in the deterministic transport solution. The reaction rates from the pointwise transport solution are condensed to few-groups, homogenized over a coarser diffusion theory cell geometry, and used to determine the initial few-group diffusion theory parameters. The few-group diffusion theory problem is solved using the diffusion theory solver of Reference 8 and the few-group reaction rates from the transport and diffusion theory solutions are compared. If the reaction rates are not within user specified criteria, the few-group diffusion theory parameters are adjusted in the fitting module.[9] Fitting/diffusion theory solution iterations are performed until the transport and diffusion theory reaction rates converge. Once diffusion theory reaction rates are converged, the fitted cell few-group diffusion theory parameters are edited using a standard file format. An optional depletion module, based on the CINDER[10] program, is also available. Our solution method requires less than 1 CPU-hour per timestep on a Cray C90 to solve a typical 2D cell problem containing approximately 12,000 mesh cells, 2325 energy points, and 144 angular ordinates.

III. METHODOLOGY

A. Pointwise Energy Transport Solution

A pointwise energy solution method is used, in both the fast and thermal energy ranges, to solve the fixed source neutron transport equation for one- and two-dimensional geometries. The solution method uses several overlapping energy mesh. They are, from the coarsest to the finest, the few-group energy mesh, the multigroup (MUFT[11] group) energy mesh, a fine solution energy mesh, and an ultra-fine cross section energy mesh. Each few-group typically contains several multigroups. Each multigroup typically contains 10s to 100s of uniformly spaced solution energy points, and there are typically 500 or 1000 uniformly spaced cross section energy points per multigroup.

Pointwise cross section data are used throughout the fast and thermal energy ranges except for inelastic scattering and the average number of neutrons emitted per fission (ν), which are represented using multigroup-averaged data. The inelastic scattering cross section is adjusted to include contributions from (n,2n) and (n,3n) reactions. At each energy point, two discrete ordinates transport solution methods are currently available for one- and two-dimensional geometries with reflecting and/or rotationally periodic boundary conditions: a weighted diamond difference method, based on the transport theory solution method of Reference 8, or the method of characteristics. A variety of single-Gauss, double-Gauss, and quadruple range[12] quadrature sets are available for both weighted diamond difference and method of characteristics solution methods. Due to computer storage considerations, the pointwise fluxes and scattering sources are currently limited to P_1 angular distributions. Spatial and spectral self-shielding effects are implicitly represented in the transport solution by the detailed spatial and energy discretizations.

1. Fast Energy Range

For two-dimensional x-y geometry, neutron transport for energy points in the fast energy range (from 0.625 eV to approximately 20 MeV) is modeled using

$$\underline{\Omega} \cdot \bar{\nabla} \Psi_n + \Sigma_{t,n} \Psi_n = \frac{1}{4\pi}[F_n + S_{0,n} + 3(\Omega_x S_{1x,n} + \Omega_y S_{1y,n})] + \frac{1}{4\pi}[\hat{S}_{0,n-1} + 3(\Omega_x \hat{S}_{1x,n-1} + \Omega_y \hat{S}_{1y,n-1})] \quad (1)$$

where the spatial and angular dependencies have been suppressed, and where Ψ_n is the angular flux for particles at energy point n moving in the direction of the unit vector $\underline{\Omega} = (\Omega_x, \Omega_y, \Omega_z)$, $\Sigma_{t,n}$ is the total macroscopic cross section at energy point n, F_n is the fission source at energy point n, $S_{0,n}$ and $S_{1u,n}$ ($u = x$ or y) are respectively the P_0 and x- and y-directed P_1 moments of the source at energy point n due to slowing down from energy points $n' < n$, and $\hat{S}_{0,n-1}$ and $\hat{S}_{1u,n-1}$ are respectively the P_0 and x- and y-directed P_1 moments of the ingroup scattering source from energy point $n-1$. The P_0 and P_1 moments of the flux for each energy point n are calculated using angular quadratures

$$\phi_n = \int_{\Omega} \Psi_n d\Omega \cong \sum_{k=1}^{4M_Q} w_k \Psi_n^k, \quad J_{u,n} = \int_{\Omega} \Omega_u \Psi_n d\Omega \cong \sum_{k=1}^{4M_Q} w_k \Omega_u^k \Psi_n^k. \quad (2)$$

Since thousands of energy points are used in the fast energy range, the solution energy intervals are sufficiently narrow so that the effect of ingroup scattering may be neglected. Consequently, the neutron flux at each energy point in the fast energy range is obtained using the purely absorbing approximation. When calculating the downscattering sources, however, the ingroup scattering component of the source is added (pushed down) to the next energy point.

A high-order equiprobable histogram elastic scattering angular distribution treatment is used for the heavy nuclides. The equiprobable histogram treatment is attractive because it can accurately represent highly forward peaked angular distributions, guarantee positivity, and is relatively efficient. For the heavy nuclides, the elastic scattering probability density function for the equiprobable histogram angular distribution treatment is given by

$$f(E,\omega) = f_k(E) = \frac{1}{\mathsf{NB}}\frac{1}{\Delta\omega_k(E)}, \text{ for } \omega \in \Delta\omega_k(E), \tag{3}$$

where NB is the number of equiprobable histograms (typically 32), ω is the cosine of the scattering angle in the center-of-mass (CM) system, $\omega_k(E)$ is the scattering angle breakpoint in the CM system for histogram k at energy E, $\Delta\omega_k(E) = \omega_k(E) - \omega_{k-1}(E)$, and $k = 1, \ldots, \mathsf{NB}$. The histogram breakpoints are organized such that $-1 = \omega_0(E) < \omega_k(E) < \omega_{\mathsf{NB}}(E) = 1$ and are generated by linearly interpolating between the pointwise elastic scattering angular distribution data. The Legendre moments of the differential elastic scattering cross section for scattering from energy point n into exit energy interval n' are determined using

$$\sigma_{es,\,l,\,n\to n'} = \sigma_{es}(E_{n-1/2}) \int_{\Delta\omega_{n'}} f(E_{n-1/2},\omega)P_l(\mu(\omega))d\omega \tag{4}$$

where $\sigma_{es}(E_{n-1/2})$ is the microscopic elastic scattering cross section at the midpoint of the solution energy interval n, μ is the cosine of the scattering angle in the Laboratory (LAB) system, $P_l(x)$ is the l-th Legendre polynomial, and $\Delta\omega_{n'}$ is the range of CM system scattering angles corresponding to exit energy interval n'. For a target at rest, the expressions for the cosine of the CM and LAB system scattering angles are given by

$$\omega(E') = \frac{1}{2A}\left[(1+A)^2\frac{E'}{E_{n-1/2}} - (1+A^2)\right], \tag{5}$$

$$\mu(\omega) = \frac{1+A\omega}{\sqrt{1+A^2+2A\omega}}, \tag{6}$$

where E' is the neutron exit energy and A is the ratio of the nuclide mass to the rest mass of a neutron. For the equiprobable histogram treatment, the integral in Equation (4) is approximated using

$$\int_{\Delta\omega_{n'}} f(E_{n-1/2},\omega)P_l(\mu(\omega))d\omega = \sum_{\Delta\omega\in\Delta\omega_{n'}}\left[\int_{\Delta\omega} f_k P_l(\mu(\omega))d\omega\right], \tag{7}$$

where $\Delta\omega$ indicates the full or partial range of the cosine of the CM system scattering angles for equiprobable histogram k. Thus, the Legendre moments of the probability of elastically scattering into exit energy interval n' consist of the sum of integrals over one or more equiprobable histograms. The integrals for the P_0 and P_1 moments may be obtained analytically using

$$\int_{\Delta\omega} f_k d\omega = \int_{\omega_2}^{\omega_1} f_k d\omega = f_k(\omega_1 - \omega_2), \tag{8}$$

$$\int_{\Delta\omega} f_k\mu(\omega)d\omega = \frac{f_k}{3A}\left\{[2-A^2+A\omega_1]\sqrt{1+A^2+2A\omega_1} - [2-A^2+A\omega_2]\sqrt{1+A^2+2A\omega_2}\right\}. \tag{9}$$

For hydrogen, elastic scattering from energy points in the fast energy range is modeled using a modified free gas scattering kernel.[13,14] Since upscattering is not permitted in the fast energy range, the ingroup scattering component is adjusted to

include the probability of upscattering. A dual energy resolution slowing down algorithm is used for hydrogen. Solution energy interval sized exit energy intervals are used for the energy points in the first few multigroups below the current energy point. Multigroup sized exit energy intervals are used for the remaining energy range. The P_0 and P_1 ingroup scattering components of the differential elastic scattering cross section are approximated by

$$\sigma^H_{es,\,0,\,n\to n} = \sigma^H_{es,\,1,\,n\to n} = \sigma^H_{es}(E_{n-1/2})\left(\frac{\Delta E_n/2 + T^{*H}}{E_{n-1/2} + T^{*H}/2}\right), \tag{10}$$

where T^{*H} is the effective source temperature of hydrogen. The P_0 and P_1 downscattering components for the fine slowing down intervals n' in the fast energy range are

$$\sigma^H_{es,\,0,\,n\to n'} = \sigma^H_{es}(E_{n-1/2})\left[\frac{\Delta E_{n'}}{E_{n-1/2} + T^{*H}/2}\right], \tag{11}$$

$$\sigma^H_{es,\,1,\,n\to n'} = \sigma^H_{es,\,0,\,n\to n'}\frac{E_{n'-1/2} - T^{*H}}{\sqrt{E_{n-1/2}}\sqrt{E_{n'-1/2}}}, \tag{12}$$

where $E_{n'-1/2}$ is the midpoint of fine slowing down interval n'. The downscattering components for the multigroup slowing down intervals m' in the fast energy range are approximated by

$$\sigma^H_{es,\,0,\,n\to m'} = \sigma^H_{es}(E_{n-1/2})\left[\frac{\Delta E_{m'}}{E_{n-1/2} + T^{*H}/2}\right], \tag{13}$$

$$\sigma^H_{es,\,1,\,n\to m'} = \sigma^H_{es,\,0,\,n\to m'}\frac{E_{m'-1/2} - T^{*H}}{\sqrt{E_{n-1/2}}\sqrt{E_{m'-1/2}}}, \tag{14}$$

where $E_{m'-1/2}$ is the midpoint of multigroup m'. The downscattering components for the multigroup slowing down intervals m' in the thermal energy range are approximated using

$$\sigma^H_{es,\,0,\,n\to m'} = \sigma^H_{es}(E_{n-1/2})\left[\frac{E_{cp} - T^{*H}/2}{E_{n-1/2} + T^{*H}/2}\right]A^H_{m'}, \tag{15}$$

$$\sigma^H_{es,\,1,\,n\to m'} = \sigma^H_{es,\,0,\,n\to m'}\frac{B^H_{m'}}{\sqrt{E_{n-1/2}}}, \tag{16}$$

where E_{cp} is the thermal cutpoint (0.625 eV) and

$$A^H_{m'} = \frac{(E_{m'-1} - E_{m'})\,\mathrm{Erf}\sqrt{E_{m'-1/2}/T^{*H}}}{\sum_{m''=M_F+1}^{M_F+M_T}(E_{m''-1} - E_{m''})\,\mathrm{Erf}\sqrt{E_{m''-1/2}/T^{*H}}}, \tag{17}$$

$$B^H_{m'} = \frac{(E_{m'-1/2} - T^{*H})}{\sqrt{E_{m'-1/2}}} + 2\sqrt{\frac{T^{*H}}{\pi}}\frac{e^{-E_{m'-1/2}/T^{*H}}}{\mathrm{Erf}\sqrt{E_{m'-1/2}/T^{*H}}}. \tag{18}$$

2. Thermal Energy Range

Neutron transport for energy points in the thermal energy range (0 to 0.625 eV) is modeled using

$$\underline{\Omega} \cdot \bar{\nabla}\Psi_n + \Sigma_{t,n}\Psi_n = \frac{1}{4\pi}[S_{0,n} + 3(\Omega_x S_{1x,n} + \Omega_y S_{1y,n})] \tag{19}$$

$$+ \frac{1}{4\pi} \sum_{n'=N_F+1}^{N_F+N_T} [\Sigma_{s0,n' \to n}\phi_{n'} + 3\Sigma_{s1,n' \to n}\{\Omega_x J_{x,n'} + \Omega_y J_{y,n'}\}]$$

where, $\Sigma_{sl,n' \to n}$ is the l-th Legendre moment of the differential scattering cross section for scattering from energy point n' to n, $S_{0,n}$ and $S_{1u,n}$ are respectively the P_0 and x- and y-directed P_1 moments of the source at thermal energy point n due to slowing down from the fast energy range, N_F is the number of energy points in the fast energy range, and N_T is the number of energy points in the thermal energy range (typically 25). Energy transfer is only permitted for nuclides with thermal scattering kernels, typically hydrogen. Since upscattering is permitted in the thermal energy range, successive overrelaxation (SOR) accelerated sub-group iterations are performed to converge the flux in the thermal energy range.

B. Slowing Down Algorithm

Computer memory and/or disk storage requirements for the slowing down calculation would be excessive for two-dimensional geometries if the fine solution energy structure were used for the slowing down sources throughout the energy domain. Our method uses a dual energy resolution slowing down algorithm which reduces the computer memory and disk storage requirements for the slowing down calculation while retaining most of the accuracy of the detailed slowing down solution. As illustrated in Figure 2, slowing down source moments are stored in two buffers: the fine slowing down buffer (FSDB) and the multigroup slowing down buffer (MSDB). The FSDB is memory resident and contains source moments for energy point-sized slowing down intervals for the energy points in a few (typically 2-4) multigroups below the current energy point. The FSDB is sized to contain the differential elastic scattering cross sections for the heavy nuclides for all energy points in the fast energy range. The size of the FSDB is a function of the atomic mass of the lightest heavy nuclide, the lethargy width of the multigroups, and the energy point structure of the solution. The MSDB contains source moments for multigroup-sized slowing down intervals and may be memory, solid state device (SSD), or disk resident.

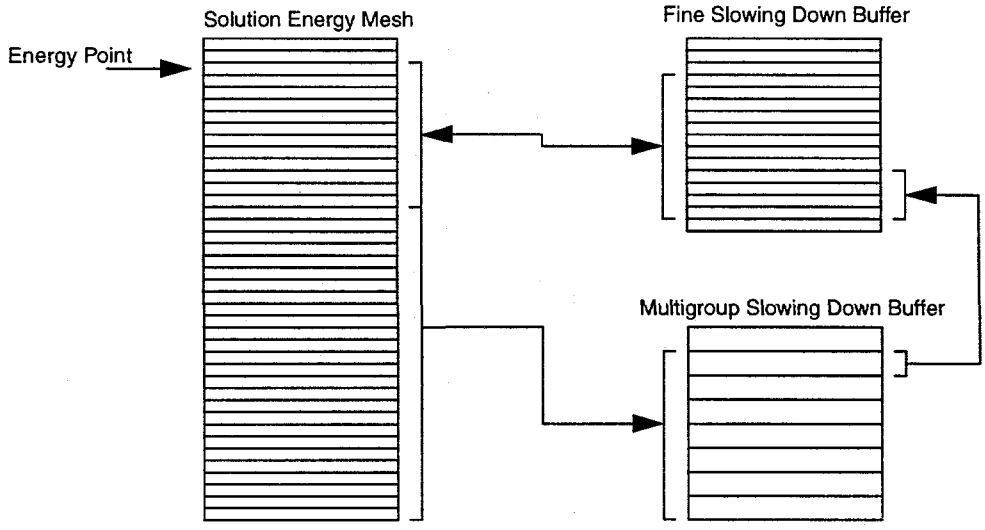

Figure 2. Dual Energy Resolution Slowing Down Algorithm

At each energy point during the slowing down calculation, the differential scattering cross sections are explicitly calculated for each nuclide. In the fast energy range, differential elastic scattering cross sections for the heavy nuclides are calculated using fine slowing down intervals. The differential inelastic scattering and hydrogen elastic scattering cross sections are calculated using a combination of fine and multigroup slowing down intervals. Fine slowing down intervals are used for the energy points contained in the FSDB, typically the energy points in a few multigroups below the current energy point, and multigroup slowing down intervals are used for the remaining slowing down energy range. As the energy solution progresses, the active size of the FSDB contracts as the source moments from previous energy points are removed from the buffer, and expands as source moments from the MSDB are moved into the FSDB. Upon entry into the thermal energy range, the source moments for energy points in the thermal energy range are moved from the MSDB into the FSDB and the calculation is continued using the FSDB.

With the dual energy resolution slowing down algorithm, the P_0 and P_1 moments of the slowing down source for energy point n are given by

$$S_{0,n} = \sum_{n'=1}^{n-1} \Sigma_{s,0,n' \to n} \phi_{n'} + \frac{1}{N_m} \sum_{n'=1}^{n-1} \Sigma_{s,0,n' \to m} \phi_{n'} \tag{20}$$

$$S_{1u,n} = \sum_{n'=1}^{n-1} \Sigma_{s,1,n' \to n} J_{u,n'} + \frac{1}{N_m} \sum_{n'=1}^{n-1} \Sigma_{s,1,n' \to m} J_{u,n'} \tag{21}$$

where $\Sigma_{s,l,n' \to n}$ is the l-th Legendre moment ($l = 0$ or 1) of the differential scattering cross section for scattering from energy point n' to fine slowing down interval n, $\Sigma_{s,l,n' \to m}$ is the l-th moment of the differential scattering cross section for scattering from energy point n' to multigroup slowing down interval m, and N_m is the number of energy points in multigroup m. Similarly, the ingroup scattering source moments for energy point n are given by

$$\hat{S}_{0,n} = \Sigma_{s,0,n \to n} \phi_n, \quad \hat{S}_{1u,n} = \Sigma_{s,1,n \to n} J_{u,n}. \tag{22}$$

IV. SAMPLE CALCULATION

Our deterministic method has been compared to Monte Carlo (RCP01) transport solutions for a BWR 1/4 pin cell depletion benchmark problem. The geometry, material, and depletion chain specifications for this problem were obtained from D. J. Kelly's BWR lattice depletion benchmark problem[15] and correspond to a fuel pin containing material 10. The geometry specifications and material specifications for this problem are provided in Figure 3 and Table 1. The x and y mesh for the deterministic solution geometry contain: 10 equally spaced mesh cells in the fuel, 2 equally spaced mesh cells in the cladding, and 5 equally spaced mesh cells in the moderator. The number densities for the meshed geometry have been adjusted to maintain material loadings. Both solutions limit the number of nuclides per depletion chain to 15. Therefore, the Gadolinium and Terbium nuclides have been neglected from the Nd-145 fission product chain. The quarter fuel pin was depleted at a linear power density of 47.6612 W/cm. 500 hour timesteps were used for the depletion calculation except at the beginning, where an initial 100 hour and 400 hour timestep was used.

The solutions for the BWR 1/4 pin cell depletion benchmark problem are presented in Tables 2 thru 4. Both calculations used the same RCPL1 pointwise cross section library with 43,300 energy points and ENDF/B-VI cross sections and fission product yields. The RCP01 results were produced by statistically combining 10 fixed source calculations per timestep, each containing 300,000 neutron histories. The deterministic calculations contained 4625 energy points, used the method of characteristics solver, a quadruple range quadrature set with 48 ordinates/octant. Due to the small size of this benchmark problem, only the transport solution was performed. Table 2 shows that the k_∞ estimates for the deterministic calculation are within the 95% confidence interval of the RCP01 Monte Carlo estimates for about half of the depletion timesteps. The maximum difference in k_∞ was 0.12% between 11,000 and 12,500 hours. Tables 3 and 4 provide the neutron balances at BOL and 17,000 hours, respectively. These results indicate that the deterministic method tends to overpredict absorption within the fuel pellet. Detailed analysis of these results indicate that a finer energy mesh, a finer spatial mesh or a higher order transport solution method, and the retention of additional Legendre moments in the angular representation of the scattering source would improve the agreement between deterministic and Monte Carlo solutions.

V. CONCLUSIONS

Deterministic transport theory methods may be used to calculate accurate transport corrected few-group diffusion theory parameters for complex one- and two-dimensional geometries. The combination of a near-continuous energy pointwise solution method and a detailed transport theory cell geometry permits the implicit treatment of spatial and spectral self-shielding effects for lattice physics problems. A dual energy resolution slowing down algorithms is used to reduce the memory requirements for two-dimensional geometries. Results from the deterministic pointwise energy solution method were compared to the RCP01 continuous energy Monte Carlo neutron transport program for a BWR 1/4 pin cell depletion benchmark problem.

VI. ACKNOWLEDGMENTS

The author would like to acknowledge the contributions of N. R. Candelore, R. C. Gast, and D. E. Dei who were responsible for the initial development of these methods. This work was supported by the U.S. Department of Energy under Contract DE-AC11-98PN38206.

VII. REFERENCES

1. C. J. Pfeifer, C. J. Spitz, "PDQ-8 Reference Manual," WAPD-TM-1266, Bettis Atomic Power Laboratory (1978).

2. M. Edenius, H. Haggblom, B. H. Forssen, "CASMO-3 Methodology Manual," STUDSVIK/NFA-89/2, Studsvik of America (1989).

3. D. B. Jones, K. E. Watkins, B. D. Paulson, "CPM-3 Computer Code Manual Vol 2: User Manual," EPRI RP-3418, Electric Power Research Institute (July 1998).

4. "WIMSD5: Deterministic Code System for Reactor-Lattice Calculations," CCC-656, Radiation Safety Information Computational Center (December 1997).

5. M. L. Williams, M. Asgari, "Computation of Continuous Energy Neutron Spectra with Discrete Ordinates Transport Theory," *Nuclear Science and Engineering*, **121**, 173 (1995).

6. A. V. Dralle, N. R. Candelore, R. C. Gast, "RCPL1 - A Program to Prepare Neutron and Photon Cross-Section Libraries for RCP01," WAPD-TM-1268, Bettis Atomic Power Laboratory (1978).

7. N. R. Candelore, L. Ondis, "RCP01 - A Monte Carlo Program for Solving the Neutron and Photon Transport Problems in Three-Dimensional Geometry with Detailed Energy Description," WAPD-TM-1267, Bettis Atomic Power Laboratory (1978).

8. I. K. Abu-Shumays, "Vectorization of Transport and Diffusion Computations on the CDC Cyber 205," *Nuclear Science and Engineering*, **92**, 4-19 (1986).

9. D. S. Rampolla, "Adjusting Absorption Cross Sections in Transport Calculations to Achieve Specified Region Capture Integrals," *Nuclear Science and Engineering*, **31**, 396-414 (1968).

10. T. R. England, "CINDER - A One-Point Depletion and Fission Product Program," WAPD-TM-334, Bettis Atomic Power Laboratory (1962).

11. H. Bohl Jr. and A. P. Hemphill, "MUFT-5, A Fast Neutron Spectrum Program for the PHILCO 2000," WAPD-TM-218, Bettis Atomic Power Laboratory (1961).

12. I. K. Abu-Shumays, "Compatible Product Angular Quadrature for Neutron Transport in x-y Geometry," *Nuclear Science and Engineering*, **64**, 299-316 (1977).

13. W. W. Clendenin, "The Monatomic Gas Model for Thermal Neutron Distributions in a Physical Moderator," *J. Nucl. Energy, Part A*, **13**, 25-34 (1960).

14. G. I. Bell and S. Glasstone, *Nuclear Reactor Theory*, Van Nostrand Reinhold, 1970.

15. D. J. Kelly, *Proceedings of the International Conference on Mathematics and Computations, Reactor Physics, and Environmental Analyses*, Portland Oregon, April 30 - May 4, 1995, Vol. 2, pp. 1011-1023, American Nuclear Society (1995).

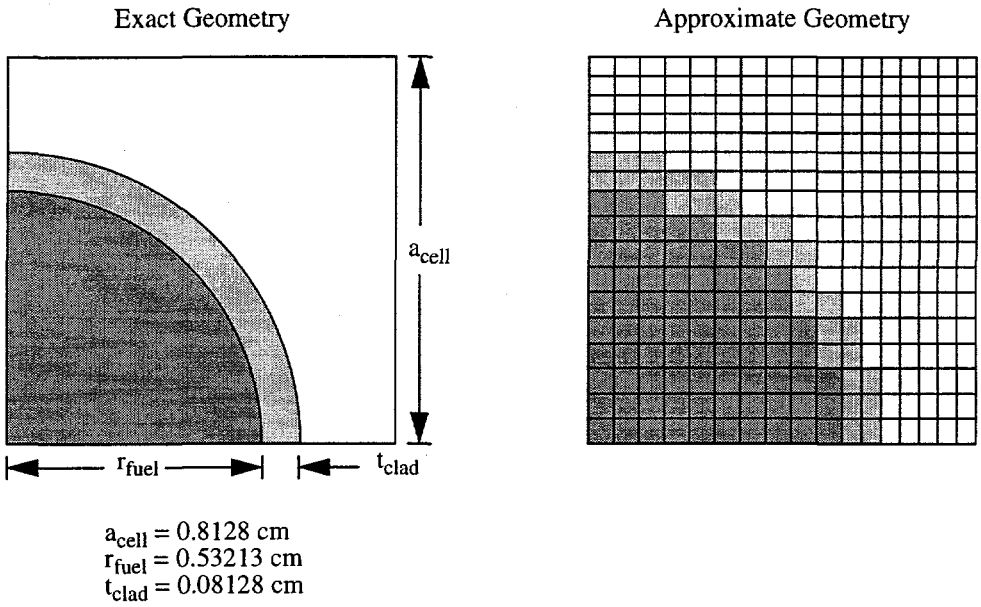

Figure 3. Geometry Specification for BWR 1/4 Pin Cell Problem

Table 1: Material Number Densities for BWR 1/4 Pin Cell at BOL for 40% Void

Material	Nuclide	Temperature (K)	Number Densities (atoms/barn-cm)	
			RCP01	Deterministic
Fuel (10)	U234	833	8.2406E-6	8.1926E-6
	U235	833	8.9783E-4	8.9260E-4
	U238	833	2.1548E-2	2.1422E-2
	O16	833	4.4908E-2	4.4646E-2
Clad (76)	Zr	600	4.3239E-2	4.4278E-2
Moderator (72-40V)	H1	600	3.05884E-2	3.05539E-2
	O16	600	1.52942E-2	1.52769E-2

Table 2: k_∞ versus Exposure

Exposure (10^3 hrs)	Deterministic k_∞	RCP01 k_∞ (95% CI)	Exposure (10^3 hrs)	Deterministic k_∞	RCP01 k_∞ (95% CI)
0.0	1.27391	1.27348 (4.36E-04)	8.5	1.13100	1.13031 (5.50E-04)
0.1	1.24019	1.23989 (5.45E-04)	9.0	1.12598	1.12529 (6.81E-04)
0.5	1.23040	1.23042 (6.37E-04)	9.5	1.12108	1.12034 (5.82E-04)
1.0	1.22280	1.22294 (7.12E-04)	10.0	1.11631	1.11609 (3.64E-04)
1.5	1.21620	1.21674 (5.86E-04)	10.5	1.11165	1.11090 (4.95E-04)
2.0	1.20963	1.21001 (8.00E-04)	11.0	1.10709	1.10595 (6.49E-04)
2.5	1.20297	1.20278 (5.93E-04)	11.5	1.10264	1.10149 (5.96E-04)
3.0	1.19628	1.19563 (6.05E-04)	12.0	1.09828	1.09762 (4.98E-04)
3.5	1.18963	1.18926 (3.95E-04)	12.5	1.09401	1.09282 (8.87E-04)
4.0	1.18307	1.18247 (3.49E-04)	13.0	1.08982	1.08902 (4.62E-04)
4.5	1.17664	1.17579 (6.75E-04)	13.5	1.08571	1.08499 (4.94E-04)
5.0	1.17036	1.16968 (4.89E-04)	14.0	1.08168	1.08077 (4.71E-04)
5.5	1.16425	1.16375 (8.38E-04)	14.5	1.07772	1.07675 (6.25E-04)
6.0	1.15831	1.15803 (5.92E-04)	15.0	1.07382	1.07337 (5.20E-04)
6.5	1.15253	1.15191 (8.41E-04)	15.5	1.06999	1.06964 (7.53E-04)
7.0	1.14692	1.14668 (7.04E-04)	16.0	1.06622	1.06535 (9.17E-04)
7.5	1.14146	1.14070 (5.40E-04)	16.5	1.06250	1.06202 (6.22E-04)
8.0	1.13616	1.13531 (4.22E-04)	17.0	1.05885	1.05797 (5.72E-04)

Table 3: Neutron Balances for BWR 1/4 Pin Cell at BOL

Region	Isotope	Type	Deterministic Reaction Rate	RCP01 Reaction Rate (95% CI)
Fuel	U234	ABS	3.0322E-03	3.0393E-03 (1.67E-05)
	U235	ABS	5.9737E-01	5.9855E-01 (3.08E-04)
	U238	ABS	3.6801E-01	3.6658E-01 (1.95E-04)
	O16	ABS	2.9928E-03	2.8414E-03 (1.08E-05)
	U234	FIS	8.3964E-05	8.1863E-05 (1.18E-07)
	U235	FIS	4.7702E-01	4.7815E-01 (2.21E-04)
	U238	FIS	3.9990E-02	3.8847E-02 (7.02E-05)
	TOTAL	ABS	9.7140E-01	9.7101E-01 (1.85E-04)
Clad	Zr	ABS	1.0265E-02	1.0420E-02 (4.24E-05)
Mod	O16	ABS	1.5877E-03	1.6198E-03 (8.75E-06)
	H1	ABS	1.8480E-02	1.8654E-02 (2.30E-05)
	TOTAL	ABS	2.0068E-02	2.0274E-02 (2.23E-05)
Cell	TOTAL	ABS	1.00174	1.00170 (1.92E-04)
	TOTAL	NU-F	1.27391	1.27348 (4.36E-04)

Table 4: Neutron Balances for BWR 1/4 Pin Cell at 17,000 Hours

Region	Isotope	Type	Deterministic Reaction Rate	RCP01 Reaction Rate (95% CI)
Fuel	U234	ABS	1.9598E-03	1.9624E-03 (9.98E-06)
	U235	ABS	2.6702E-01	2.6769E-01 (1.89E-04)
	U236	ABS	8.2802E-03	8.2895E-03 (4.64E-05)
	U238	ABS	3.4730E-01	3.4556E-01 (3.73E-04)
	NP237	ABS	1.9368E-03	1.9494E-03 (6.62E-06)
	NP239	ABS	3.9828E-04	3.9858E-04 (7.91E-07)
	PU238	ABS	1.9553E-04	1.9808E-04 (6.56E-07)
	PU239	ABS	2.1585E-01	2.1624E-01 (2.51E-04)
	PU240	ABS	4.7172E-02	4.7309E-02 (2.02E-04)
	PU241	ABS	2.0609E-02	2.0734E-02 (1.25E-05)
	PU242	ABS	2.8644E-03	2.9036E-03 (2.70E-05)
	AM241	ABS	4.8937E-04	4.8928E-04 (8.95E-07)
	AM242M	ABS	3.5525E-05	3.5877E-05 (3.01E-08)
	AM243	ABS	5.7259E-04	5.8061E-04 (3.02E-06)
	CM242	ABS	5.1070E-06	5.0044E-06 (3.73E-08)
	CM244	ABS	3.2444E-05	3.2913E-05 (3.41E-07)
	KR83	ABS	3.3250E-04	3.3359E-04 (2.12E-06)
	MO99	ABS	2.7801E-06	2.7817E-06 (3.10E-09)
	TC99	ABS	2.9072E-03	2.9169E-03 (1.83E-05)
	RU101	ABS	1.4110E-03	1.4162E-03 (5.72E-06)
	RU103	ABS	7.1712E-05	7.1755E-05 (1.13E-07)
	RU105	ABS	2.9974E-08	2.9906E-08 (2.65E-11)
	RH103	ABS	6.3026E-03	6.3224E-03 (2.25E-05)
	RH015	ABS	3.5343E-04	3.5452E-04 (5.64E-07)
	PD015	ABS	6.2166E-04	6.1895E-04 (2.04E-06)
	CD113	ABS	1.7533E-04	1.7551E-04 (3.49E-07)
	I131	ABS	1.3848E-06	1.3831E-06 (2.12E-09)
	I135	ABS	2.9333E-10	2.9325E-10 (1.72E-13)
	XE131	ABS	4.8976E-03	4.8712E-03 (3.03E-05)
	XE133	ABS	7.8858E-05	7.9176E-05 (8.01E-08)
	XE135	ABS	1.2685E-02	1.2727E-02 (1.80E-05)
	CS133	ABS	4.1614E-03	4.1658E-03 (1.15E-05)
	CS134	ABS	1.7066E-04	1.7216E-04 (2.07E-07)
	CS135	ABS	4.7341E-04	4.7318E-04 (5.60E-07)
	PR143	ABS	8.2610E-05	8.2955E-05 (1.03E-07)
	ND143	ABS	4.0777E-03	4.1082E-03 (5.92E-06)
	ND145	ABS	1.8557E-03	1.8635E-03 (1.05E-05)
	ND146	ABS	3.9413E-05	3.9385E-05 (1.93E-07)
	ND147	ABS	9.9327E-05	1.0264E-04 (1.71E-07)
	ND148	ABS	7.9769E-05	7.9699E-05 (5.02E-07)
	PM147	ABS	3.8092E-03	3.7956E-03 (1.66E-05)
	PM148M	ABS	1.0853E-03	1.0878E-03 (3.12E-06)

Table 4: Neutron Balances for BWR 1/4 Pin Cell at 17,000 Hours (Continued)

Region	Isotope	Type	Deterministic Reaction Rate	RCP01 Reaction Rate (95% CI)
	PM149	ABS	2.8114E-05	2.8261E-05 (1.88E-08)
	PM151	ABS	6.2534E-06	6.2679E-06 (6.65E-09)
	SM147	ABS	5.8277E-04	5.8287E-04 (2.06E-06)
	SM148	ABS	5.9336E-05	5.9075E-05 (4.81E-07)
	SM149	ABS	5.8723E-03	5.8736E-03 (1.30E-05)
	SM150	ABS	5.8396E-04	5.8449E-04 (1.43E-06)
	SM151	ABS	2.6831E-03	2.6829E-03 (2.90E-06)
	SM152	ABS	1.6469E-03	1.6488E-03 (1.16E-05)
	EU153	ABS	1.0668E-03	1.0703E-03 (2.69E-06)
	EU154	ABS	5.1545E-04	5.1993E-04 (7.26E-07)
	EU155	ABS	8.2498E-04	8.2441E-04 (3.09E-06)
	EU156	ABS	2.7384E-05	2.7613E-05 (3.75E-08)
	O16	ABS	3.0030E-03	2.8429E-03 (1.07E-05)
	U234	FIS	6.0797E-05	5.9182E-05 (7.09E-08)
	U235	FIS	2.0778E-01	2.0841E-01 (1.46E-04)
	U236	FIS	3.8006E-04	3.7240E-04 (7.32E-07)
	U238	FIS	3.9561E-02	3.8350E-02 (6.15E-05)
	NP237	FIS	3.8785E-05	3.7793E-05 (8.91E-08)
	PU238	FIS	2.3599E-05	2.3959E-05 (7.32E-08)
	PU239	FIS	1.3697E-01	1.3723E-01 (1.49E-04)
	PU240	FIS	2.9848E-04	2.8948E-04 (3.95E-07)
	PU241	FIS	1.5473E-02	1.5563E-02 (9.35E-06)
	PU242	FIS	4.1876E-05	4.1025E-05 (5.71E-08)
	TOTAL	ABS	9.7739E-01	9.7699E-01 (7.36E-05)
Clad	Zr	ABS	9.5421E-03	9.6860E-03 (4.18E-05)
Mod	O16	ABS	1.5930E-03	1.6224E-03 (7.71E-06)
	H1	ABS	1.3191E-02	1.3366E-02 (1.59E-05)
	TOTAL	ABS	1.4784E-02	1.4988E-02 (1.66E-05)
Cell	TOTAL	ABS	1.00172	1.00167 (7.14E-05)
	TOTAL	NU-F	1.05885	1.05797 (5.72E-04)